https://doi.org/10.1016/j.epsr.2022.108553

Analytical Characterization of DFIG Response to Asymmetrical Voltage Dips for Efficient Design

Yuanzhu Chang, Jean Mahseredjian
Department of Electrical Engineering
Polytechnique Montréal
Montréal, Canada
yuanzhu.chang@polymtl.ca, jean.mahseredjian@polymtl.ca

Ilhan Kocar, Ulas Karaagac
Department of Electrical Engineering
The Hong Kong Polytechnic University
Hong Kong SAR
ilhan.kocar@polymtl.ca

***Abstract*—The fault current characteristics of Doubly Fed Induction Generator (DFIG) based wind turbine generator (WTGs) differ from those of traditional generators. Although asymmetrical faults are far more frequent, the studies on transient current characteristics of DFIG-based WTGs are mainly focused on symmetrical faults and consider the variations in voltage magnitude only. This paper presents highly accurate and concise analytical expressions for the stator and rotor currents of DFIG-based WTGs under crowbar protection considering the variations in magnitude and phase angle of both the positive- and negative-sequence voltages during asymmetrical faults. The proposed expressions are validated using a detailed simulation model of a 1.5MW DFIG-based WTG. The expressions can be directly integrated into protection tools for the evaluation of dynamic performance of relays and design of fault ride through (FRT) solutions.**

***Index Terms*—Doubly Fed Induction Generator (DFIG), crowbar, short circuit current, unsymmetrical fault, unbalanced voltage.**

I. INTRODUCTION

Doubly Fed Induction Generator (DFIG) based wind turbine generators (WTGs) have been playing a key role in integrating wind energy resources into modern power systems. The fault current characteristics of DFIG-based WTGs are quite different from those of well-studied synchronous generators (SGs) and needs to be characterized correctly since legacy protection elements set under the assumption of SG based generation may not function as desired under the influence of DFIG-based WTGs [1]-[4]. Moreover, the characteristics of the rotor current are also important for optimizing fault ride through (FRT) solutions to comply with different grid code requirements [5], [6].

Due to the non-full-size converters, crowbar circuit is typically employed in DFIG-based WTGs to protect the converters from overvoltages and overcurrents caused by voltage dips. Under asymmetrical faults on the power grid, the negative-sequence stator voltage generates a severe rotor electromotive force (EMF) that does not decay and that is much greater than the EMF seen during symmetrical voltage dips [7]. Consequently, the crowbar circuit is more likely to be triggered under asymmetrical voltage dips [8]. This paper focuses on DFIG response under crowbar protection.

The fault current of the DFIG-based WTGs has been studied using different approaches. Electromagnetic transient (EMT) simulations are used to study and compare the fault currents of DFIG-based WTGs and SGs in the time domain [9], [10]. Analytical studies are performed to analyze the transient and steady-state currents under different FRT control strategies and crowbar protection [11]-[15]. To the best of the authors' knowledge, the above studies consider mainly symmetrical voltage dips. For asymmetrical voltage dips and crowbar protection, the DFIG-based WTGs are simply regarded as squirrel-cage induction generators and fixed impedances in the sequence domain and short circuit calculations. However, this simplification is not accurate because of the considerable crowbar resistance and slip [16]. Detailed analytical expressions for the stator current are then proposed in [17]-[18] for asymmetrical voltage dips and crowbar protection. However, the impact of jumps in phase angle has not been studied as outlined in [19]. Moreover, the resulting expression is still complex and challenging to integrate into practical short circuit packages and relaying applications.

To fill the gap of research regarding the DFIG's characterization under transient asymmetrical fault conditions and crowbar protection, this paper extends the analytical method proposed in [14] to asymmetrical voltage dips and proposes practical expressions for the stator and rotor currents by fully considering the variations in magnitude and jumps in phase angle of both the positive- and negative-sequence voltages during asymmetrical voltage dips. This paper then develops the transient, positive-sequence and negative-sequence equivalent stator inductances of DFIG-based WTGs. The concept of equivalent inductance helps developing concise expressions suitable for protection studies and FRT design.

The rest of the paper is organized as follows. Section II presents the magnitude and phase angle characteristics of asymmetrical voltage dips. Section III reorganizes the basic equations governing the DFIG dynamics, and then derives the

Submitted to the 22nd Power Systems Computation Conference (PSCC 2022).

expression of equivalent inductance. By further identifying the specific equivalent stator inductances for transient, positive- and negative-sequence components, Section IV proposes the stator and rotor expressions. Section V validates the analytical expressions with time domain simulations using a detailed model. Finally, conclusions are drawn in Section VI.

II. Asymmetrical Voltage Dip Characteristics

Stator is the point of connection of a DFIG-based WTG. Its voltage before and after an asymmetrical voltage dip is mathematically characterized in this section.

A. Characteristics of Asymmetrical Voltage Dip

Fig. 1 shows the waveform of an asymmetrical voltage dip triggering crowbar protection. It is observed that, after the voltage dip, the transient components are not significant and thus the voltage of each phase mainly consists of the fundamental frequency component [20]. The three-phase voltages before and after the dip are then generically given by:

$$\begin{aligned} u_a &= U_a \cos(\omega_1 t + \theta_a) \\ u_b &= U_b \cos(\omega_1 t + \theta_b) \\ u_c &= U_c \cos(\omega_1 t + \theta_c) \end{aligned} \tag{1}$$

where u stands for the instantaneous voltage, U stands for the peak voltage magnitude. ω_1 is the angular velocity of the grid voltage, θ is the phase angle, and subscripts a, b and c stand for the phase.

Since zero-sequence voltages and currents are isolated by WP and WTG transformers, the three-phase stator voltage can be represented with the positive- and negative-sequence components by applying the method of symmetrical components as follows

$$\begin{bmatrix} U_+ e^{j\theta_+} \\ U_- e^{j\theta_-} \end{bmatrix} = \frac{1}{3} \begin{bmatrix} 1 & e^{j\frac{2\pi}{3}} & e^{-j\frac{2\pi}{3}} \\ 1 & e^{-j\frac{2\pi}{3}} & e^{j\frac{2\pi}{3}} \end{bmatrix} \begin{bmatrix} U_a e^{j\theta_a} \\ U_b e^{j\theta_b} \\ U_c e^{j\theta_c} \end{bmatrix}. \tag{2}$$

where the subscripts + and – indicate positive- and negative-sequence components, respectively.

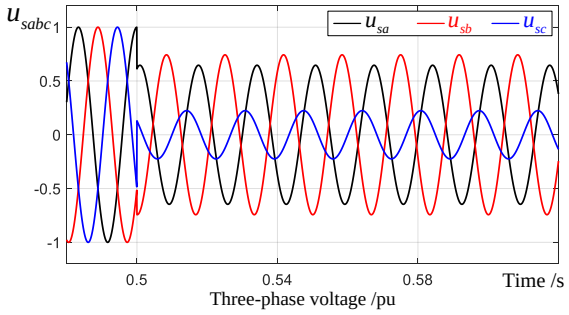

Figure 1. Voltage waveform before and after an asymmetrical voltage dip.

Before the voltage dip, the stator voltage consists of only a positive-sequence component. The stator voltage can be expressed with complex vector (represented in italic and bold characters) [21] in the two-phase stationary reference frame (denoted by $\alpha\beta$) as follows

$$\boldsymbol{U}_{s\ \mathrm{pre}}^{\alpha\beta} = u_\alpha + j u_\beta = \boldsymbol{U}_{s+\ \mathrm{pre}}^{dq+} e^{j\omega_1 t} \tag{3}$$

where

$$\boldsymbol{U}_{s+\ \mathrm{pre}}^{dq+} = U_{+\ \mathrm{pre}} e^{j\theta_{+\ \mathrm{pre}}} \tag{4}$$

$$\begin{bmatrix} u_\alpha \\ u_\beta \end{bmatrix} = \frac{2}{3} \begin{bmatrix} 1 & -\frac{1}{2} & -\frac{1}{2} \\ 0 & \frac{\sqrt{3}}{2} & -\frac{\sqrt{3}}{2} \end{bmatrix} \cdot \begin{bmatrix} u_a \\ u_b \\ u_c \end{bmatrix} \tag{5}$$

In this paper, the subscript pre and post indicate values before and after the voltage dip. Subscript s stands for stator. The superscripts $\alpha\beta$, $dq+$ and $dq-$ indicate that the vector is measured with respect to the $\alpha\beta$ frame, two-phase synchronous reference frame rotating with ω_1 and two-phase synchronous reference frame rotating with $-\omega_1$, respectively.

After the voltage dip, the stator voltage vector consists of the positive- and negative-sequence components

$$\boldsymbol{U}_{s\ \mathrm{post}}^{\alpha\beta} = \boldsymbol{U}_{s+\ \mathrm{post}}^{\alpha\beta} + \boldsymbol{U}_{s-\ \mathrm{post}}^{\alpha\beta} = \boldsymbol{U}_{s+\ \mathrm{post}}^{dq+} e^{j\omega_1 t} + \boldsymbol{U}_{s-\ \mathrm{post}}^{dq-} e^{-j\omega_1 t} \tag{6}$$

where

$$\boldsymbol{U}_{s+\ \mathrm{post}}^{dq+} = U_{+\ \mathrm{post}} e^{j\theta_{+\ \mathrm{post}}} \quad \boldsymbol{U}_{s-\ \mathrm{post}}^{dq-} = U_{-\ \mathrm{post}} e^{-j\theta_{-\ \mathrm{post}}} \tag{7}$$

where the complex vector expression of the negative-sequence components is detailed in [22].

Compared with the pre- and post-fault stator voltage vectors in (3) and (7), the asymmetrical voltage dip can be regarded as the sum of a positive-sequence voltage dip and a negative-sequence voltage step. Note that, at the instant of an asymmetrical dip, not only the magnitudes but also the phase angles of the positive- and negative-sequence voltage components change. These characteristics are also described as magnitude sags and phase angle jumps in [23].

B. Subsystems

With the assumption of a linear magnetic circuit, a DFIG-based WTG becomes a linear system following the operation of crowbar protection. Hence, the principle of superposition is applied below to decompose the complete response into two responses to simplify the calculations.

Based on the discussion on asymmetrical voltage dips in Section II.A, two subsystems are proposed from the perspective of superposition, as shown in Fig. 2.

Subsystem $S1$ is employed to obtain the response of a DFIG-based WTG to the positive-sequence voltage vector dip:

$$\boldsymbol{U}_{s.S1}^{dq+} = \begin{cases} U_{+\ \mathrm{pre}} e^{j\theta_{+\mathrm{pre}}} & \text{pre-fault} \\ U_{+\ \mathrm{post}} e^{j\theta_{+\mathrm{post}}} & \text{post-fault} \end{cases} \tag{8}$$

Subsystem $S2$ is employed to obtain the response of a DFIG-based WTG to the negative-sequence voltage step:

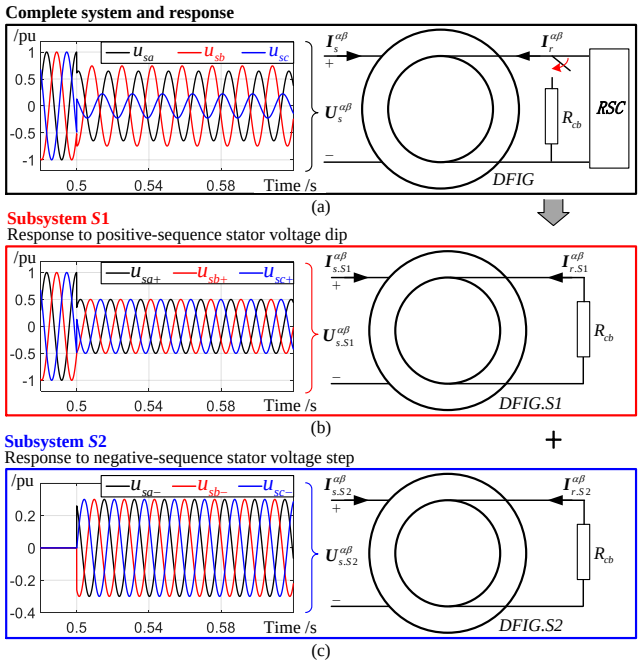

Figure 2. Complete system and subsystems; complete and decomposed responses of a DFIG-based WTG to an asymmetrical voltage dip.

$$\boldsymbol{U}_{s.S2}^{dq-}=\begin{cases}0 & \text{pre-fault}\\ U_{-\,\text{post}}e^{-j\theta_{-\,\text{post}}} & \text{post-fault}\end{cases} \tag{9}$$

The complete stator and rotor currents are the sum of the responses of these two subsystems, namely

$$\boldsymbol{I}_s^{\alpha\beta}=\boldsymbol{I}_{s.S1}^{\alpha\beta}+\boldsymbol{I}_{s.S2}^{\alpha\beta}\quad \boldsymbol{I}_r^{\alpha\beta}=\boldsymbol{I}_{r.S1}^{\alpha\beta}+\boldsymbol{I}_{r.S2}^{\alpha\beta} \tag{10}$$

III. DFIG Equations and Equivalent Inductance

Following an asymmetrical voltage dip, multiple current and flux linkage components, rotating at different angular velocities, will be induced. The equivalent inductance in [14] provides a simple approach to quantify the relationship between flux linkages and current components. This section briefly introduces the basic equations of the DFIG governing its magnetic and electric circuits and derives the expression of its equivalent inductance under crowbar protection.

A. Basic Equations of the DFIG

The basic equations governing the magnetic circuit of the DFIG are

$$\begin{aligned}\boldsymbol{\psi}_s&=L_s\boldsymbol{I}_s+L_m\boldsymbol{I}_r\\ \boldsymbol{\psi}_r&=L_m\boldsymbol{I}_s+L_r\boldsymbol{I}_r\end{aligned} \tag{11}$$

where $\boldsymbol{I}$ and $\boldsymbol{\psi}$ stand for current and flux linkage vectors, respectively. Subscripts s and r stands for rotor. L_s, L_r and L_m stand for the stator, rotor, and magnetizing inductances of the DFIG, respectively.

The stator and rotor leakage inductances (L_{ls} and L_{lr}) and the leakage factor (σ) of the DFIG are

$$\begin{aligned}L_{ls}&=L_s-L_m\\ L_{lr}&=L_r-L_m\end{aligned}\quad \sigma=1-\frac{L_m{}^2}{L_sL_r} \tag{12}$$

Substituting (12) into (11) results in.

$$\boldsymbol{\psi}_r=\frac{L_m}{L_s}\boldsymbol{\psi}_s+\sigma L_r\boldsymbol{I}_r \tag{13}$$

According to (11), the stator current can be represented with the stator flux linkage and rotor current by

$$\boldsymbol{I}_s=\frac{\boldsymbol{\psi}_s}{L_s}-\frac{L_m}{L_s}\boldsymbol{I}_r\quad \boldsymbol{I}_r=\frac{\boldsymbol{\psi}_s}{L_m}-\frac{L_s}{L_m}\boldsymbol{I}_s \tag{14}$$

The relationships between the flux linkages and currents in (11), (13) and (14) are all independent of the reference frame.

The differential equations governing the electric circuit of the DFIG are

$$\begin{aligned}\boldsymbol{U}_s^{\alpha\beta}&=R_s\boldsymbol{I}_s^{\alpha\beta}+\frac{d\boldsymbol{\psi}_s^{\alpha\beta}}{dt}\\ \boldsymbol{U}_r^{\alpha\beta}&=R_r\boldsymbol{I}_r^{\alpha\beta}-j\omega_r\boldsymbol{\psi}_r^{\alpha\beta}+\frac{d\boldsymbol{\psi}_r^{\alpha\beta}}{dt}\end{aligned} \tag{15}$$

where ω_r is the angular frequency of the rotor. R_s and R_r are the stator and rotor resistances.

During crowbar protection, the rotor voltage with the motor convention is given by

$$\boldsymbol{U}_r^{\alpha\beta}=-R_{cb}\boldsymbol{I}_r^{\alpha\beta} \tag{16}$$

where R_{cb} is the crowbar resistance in per unit.

By substituting (13) and (16) into (15), the differential equation of the rotor electric circuit can be rewritten as

$$\boldsymbol{E}_r^{\alpha\beta}=R_{re}\boldsymbol{I}_r^{\alpha\beta}-\sigma L_r\left(j\omega_r\boldsymbol{I}_r^{\alpha\beta}-\frac{d\boldsymbol{I}_r^{\alpha\beta}}{dt}\right) \tag{17}$$

where

$$\boldsymbol{E}_r^{\alpha\beta}=\frac{L_m}{L_s}\left(j\omega_r\boldsymbol{\psi}_s^{\alpha\beta}-\frac{d\boldsymbol{\psi}_s^{\alpha\beta}}{dt}\right) \tag{18}$$

$$R_{re}=R_r+R_{cb} \tag{19}$$

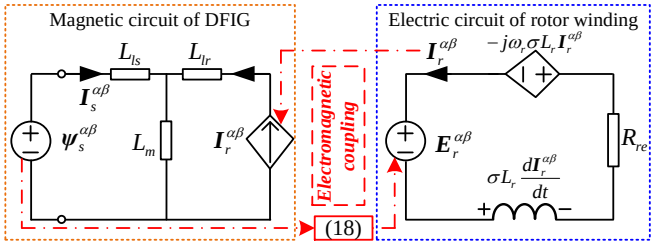

Figure 3. Electromagnetic coupling relationship between stator and rotor windings of DFIG-based WTG.

The relationship between the magnetic circuit and electric circuit of the DFIG is reorganized in Fig. 3. Due to the

electromagnetic coupling, solving these differential equations would be complex. The following section introduces equivalent inductances to obtain concise solutions with high accuracy.

B. Equivalent DFIG Inductance Considering Crowbar

Consider a single stator flux linkage component that rotates at a certain angular velocity ω_f with respect to the stator winding given by

$$\boldsymbol{\psi}_s^{\alpha\beta} = \psi_f e^{j\theta_f} \cdot e^{j\omega_f t} \tag{20}$$

where ψ_f and θ_f indicate the magnitude and phase angle of the given stator flux linkage component, respectively.

The stator flux linkage component is relatively stationary with respect to the two-phase reference frame rotating at ω_f (denoted as *dqf*), i.e.,

$$\boldsymbol{\psi}_s^{dqf} = \boldsymbol{\psi}_s^{\alpha\beta} e^{-j\omega_f t} = \psi_f e^{j\theta_f} \tag{21}$$

The rotor equation in (17) and (18) can be transformed into the *dqf* reference frame as follows

$$\boldsymbol{E}_r^{dqf} = R_{re}\boldsymbol{I}_r^{dqf} - \sigma L_r[\, j(\omega_r - \omega_f)\boldsymbol{I}_r^{dqf} - d\boldsymbol{I}_r^{dqf} / dt] \tag{22}$$

$$\boldsymbol{E}_r^{dqf} = (L_m / L_s)[\, j(\omega_r - \omega_f)\boldsymbol{\psi}_s^{dqf} - d\boldsymbol{\psi}_s^{dqf} / dt] \tag{23}$$

Since the given stator flux linkage component is stationary with respect to the *dqf* frame, the differential terms in (22) and (23) can be neglected. And the rotor current component can be solved as

$$\boldsymbol{I}_r^{dqf} = \frac{L_m}{L_s}\frac{j(\omega_r - \omega_f)\boldsymbol{\psi}_s^{dqf}}{R_{re} - j(\omega_r - \omega_f)\sigma L_r} = [1 - \frac{L_s}{\boldsymbol{L}_{eqs}(\omega_f)}]\frac{\boldsymbol{\psi}_s^{dqf}}{L_m} \tag{24}$$

By further substituting (24) into (14), the stator current component caused by the stator flux linkage component is

$$\boldsymbol{I}_s^{dqf} = \frac{\boldsymbol{\psi}_s^{dqf}}{\boldsymbol{L}_{eqs}(\omega_f)} \tag{25}$$

where

$$\boldsymbol{L}_{eqs}(\omega_f) = L_s \frac{R_{re} - j(\omega_r - \omega_f)\sigma L_r}{R_{re} - j(\omega_r - \omega_f)L_r} \tag{26}$$

This indicates that the stator and rotor current components caused by the stator flux linkage component can be approximatively calculated by the stator equivalent inductance in one step. This successfully simplifies the solution of the differential equations in (15). Moreover, (26) indicates that the equivalent stator inductance varies according to the angular velocity ω_f.

IV. Flux Linkage and Current Components

Based on the characteristics of asymmetrical voltage dips summarized in Section II, this section first identifies the stator flux linkage components and their angular velocities. Then, the stator and rotor current components corresponding to these stator flux linkage components are determined by using the equivalent stator inductance deduced in Section III. Finally, the expressions of the stator and rotor currents are found.

A. Stator Flux Linkage Components

For the positive-sequence voltage dip in subsystem *S*1, the stator flux linkage components have been studied in [7] and [24]. It is shown that the stator flux linkage consists of two components, namely the positive-sequence steady-state component and a DC transient component. The positive-sequence steady-state component rotates at ω_1 with respect to the $\alpha\beta$ frame. The DC transient component is stationary to the $\alpha\beta$ frame and its magnitude would naturally decay with a certain time constant (denoted as T_{eqs}). Consequently, the stator flux linkage vector of subsystem *S*1 is

$$\boldsymbol{\psi}_{s.S1}^{\alpha\beta} = \boldsymbol{\psi}_{s+.S1}^{dq+} e^{j\omega_1 t} + \boldsymbol{\psi}'^{\alpha\beta}_{s.S1} e^{-\frac{t}{T_{eqs}}} \tag{27}$$

where ' indicates the transient component and

$$\boldsymbol{\psi}_{s+.S1}^{dq+} = \frac{\boldsymbol{U}_{s+\text{ post}}^{dq+}}{j\omega_1} = \frac{U_{+\text{ post}} e^{j\theta_{+\text{ post}}}}{j\omega_1} \tag{28}$$

$$\boldsymbol{\psi}'^{\alpha\beta}_{s.S1} = \boldsymbol{\psi}_{s\text{ pre}}^{dq+} - \boldsymbol{\psi}_{s+.S1}^{dq+} = \frac{\boldsymbol{U}_{s+\text{ pre}}^{dq+} - \boldsymbol{U}_{s+\text{ post}}^{dq+}}{j\omega_1} \tag{29}$$

Similarly, for the negative-sequence voltage step in subsystem *S*2, the stator flux linkage is also composed of two components, namely the negative-sequence steady-state component and a DC transient component. The negative-sequence steady-state component rotates at -ω_1 with respect to the $\alpha\beta$, while the DC transient component is also stationary to the $\alpha\beta$ frame and has the same time constant in (27). The stator flux linkage of subsystem *S*2 is

$$\boldsymbol{\psi}_{s.S2}^{\alpha\beta} = \boldsymbol{\psi}_{s-.S2}^{dq-} e^{j\omega_1 t} + \boldsymbol{\psi}'^{\alpha\beta}_{s.S2} \tag{30}$$

where

$$\boldsymbol{\psi}_{s-.S2}^{dq-} = \frac{\boldsymbol{U}_{s-\text{ post}}^{dq-}}{-j\omega_1} \quad \boldsymbol{\psi}'^{\alpha\beta}_{s.S2} = -\boldsymbol{\psi}_{s-.S2}^{dq-} \tag{31}$$

By combining (27) and (30), the complete stator flux linkage is written as a combination of three components, the positive-sequence, negative-sequence and DC transient:

$$\boldsymbol{\psi}_s^{\alpha\beta} = \boldsymbol{\psi}_{s+.S1}^{dq+} e^{j\omega_1 t} + \boldsymbol{\psi}_{s-.S2}^{dq-} e^{-j\omega_1 t} + (\boldsymbol{\psi}'^{\alpha\beta}_{s.S1} + \boldsymbol{\psi}'^{\alpha\beta}_{s.S2}) e^{-\frac{t}{T_{eqs}}} \tag{32}$$

B. Stator Current Components

By substituting the angular velocity of each stator flux linkage component into (26), three specific equivalent stator inductances can be determined. First, the positive-sequence equivalent stator inductance is

$$\boldsymbol{L}_{eqs+} = \frac{\boldsymbol{\psi}_{s+.S1}^{dq+}}{\boldsymbol{I}_{s+.S1}^{dq+}} = \boldsymbol{L}_{eqs}(\omega_f = \omega_1) = L_s \frac{R_{re} + js\omega_1\sigma L_r}{R_{re} + js\omega_1 L_r} \tag{33}$$

Second, the negative-sequence equivalent stator inductance is

$$\boldsymbol{L}_{eqs-}=\frac{\boldsymbol{\psi}_{s-.S2}^{dq-}}{\boldsymbol{I}_{s-.S2}^{dq-}}=\boldsymbol{L}_{eqs}(\omega_f=-\omega_1)=L_s\frac{R_{re}+j(s-2)\omega_1\sigma L_r}{R_{re}+j(s-2)\omega_1 L_r} \quad (34)$$

Third, the transient equivalent stator inductance is

$$\boldsymbol{L}'_{eqs}=\frac{\boldsymbol{\psi}'^{\alpha\beta}_{s.S1}+\boldsymbol{\psi}'^{\alpha\beta}_{s.S2}}{\boldsymbol{I}'^{\alpha\beta}_{s.S1}+\boldsymbol{I}'^{\alpha\beta}_{s.S2}}=\boldsymbol{L}_{eqs}(\omega_f=0)=L_s\frac{R_{re}+j(s-1)\omega_1\sigma L_r}{R_{re}+j(s-1)\omega_1 L_r} \quad (35)$$

where *s* stands for the slip and is given by

$$s=(\omega_1-\omega_r)/\omega_1 \quad (36)$$

Using (33), (34) and (35), the positive-sequence, negative-sequence and DC transient components of the stator current are respectively obtained as

$$\boldsymbol{I}_{s+}^{dq+}=\boldsymbol{U}_{s+\text{ post}}^{dq+}/\,j\omega_1\boldsymbol{L}_{eqs+} \quad (37)$$

$$\boldsymbol{I}_{s-}^{dq-}=\boldsymbol{U}_{s-\text{ post}}^{dq-}/(-j\omega_1\boldsymbol{L}_{eqs-}) \quad (38)$$

$$\boldsymbol{I}'^{\alpha\beta}_{s}=(\boldsymbol{U}_{s+\text{ pre}}^{dq+}-\boldsymbol{U}_{s+\text{ post}}^{dq+}+\boldsymbol{U}_{s-\text{ post}}^{dq-})/\,j\omega_1\boldsymbol{L}'_{eqs} \quad (39)$$

In addition to these three components, another transient component that is relatively stationary to the rotor winding (called the rotor frequency transient component) will be induced to keep the stator current constant before and after the instant of voltage dip. Its time constant is denoted by T_{eqr}. In the two-phase reference frame rotating with ω_r (denoted by $\alpha\beta r$), the rotor frequency transient component of the stator current can be expressed as

$$\boldsymbol{I}'^{\alpha\beta r}_{s}=\boldsymbol{I}_{s+\text{ pre}}^{dq+}-\boldsymbol{I}_{s+}^{dq+}-\boldsymbol{I}_{s-}^{dq-}-\boldsymbol{I}'^{\alpha\beta}_{s} \quad (40)$$

The initial stator current before the asymmetrical voltage dip can be determined by the pre-fault active power reference P^*, reactive power reference Q^* and slip. The active powers provided by the stator and grid side converter are naturally assigned according to the slip. The reactive power is mainly contributed by the stator winding. Thus, the pre-fault stator current can be predicted as

$$\boldsymbol{I}_{s+\text{ pre}}^{dq+}=(\frac{-1}{1-s}\frac{P^*}{U_{+\text{ pre}}}+j\frac{Q^*}{U_{+\text{ pre}}})e^{j\theta_{+\text{ pre}}} \quad (41)$$

The damping and frequency deviation characteristics of these two transient components are studied in [14], and they can be simply represented with

$$T_{eqs}=\boldsymbol{L}'_{eqs}/R_s \quad T_{eqr}=\sigma L_r/R_r \quad (42)$$

C. Proposed Current Expressions

According to the stator current components shown in Section IV B, the expression of the complete stator current is written as follows

$$\boldsymbol{I}_s^{\alpha\beta}=\boldsymbol{I}_{s+}^{dq+}e^{j\omega_1 t}+\boldsymbol{I}_{s-}^{dq-}e^{-j\omega_1 t}+\boldsymbol{I}'^{\alpha\beta}_{s}e^{-\frac{t}{T_{eqs}}}+\boldsymbol{I}'^{\alpha\beta r}_{s}e^{-\frac{t}{T_{eqr}}+j\omega_r t} \quad (43)$$

Per (24) and (14), the rotor current expression can be obtained as

$$\boldsymbol{I}_r^{\alpha\beta}=\boldsymbol{I}_{r+}^{dq+}e^{j\omega_1 t}+\boldsymbol{I}_{r-}^{dq-}e^{-j\omega_1 t}+\boldsymbol{I}'^{\alpha\beta}_{r}e^{-\frac{t}{T_{eqs}}}+\boldsymbol{I}'^{\alpha\beta r}_{r}e^{-\frac{t}{T_{eqr}}+j\omega_r t} \quad (44)$$

where

$$\boldsymbol{I}_{r+}^{dq+}=(1-\frac{L_s}{\boldsymbol{L}_{eqs+}})\frac{\boldsymbol{\psi}_{s+.S1}^{dq+}}{L_m} \quad \boldsymbol{I}_{r-}^{dq-}=(1-\frac{L_s}{\boldsymbol{L}_{eqs-}})\frac{\boldsymbol{\psi}_{s-S2}^{dq-}}{L_m} \quad (45)$$

$$\boldsymbol{I}'^{\alpha\beta}_{r}=(1-\frac{L_s}{\boldsymbol{L}'_{eqs}})\frac{\boldsymbol{\psi}'^{\alpha\beta}_{s.S1}+\boldsymbol{\psi}'^{\alpha\beta}_{s.S2}}{L_m} \quad \boldsymbol{I}'^{\alpha\beta r}_{r}=-\frac{L_s}{L_m}\boldsymbol{I}'^{\alpha\beta r}_{s} \quad (46)$$

The rotor current measured at the rotor ports can be obtained by transforming (44) into $\alpha\beta r$ frame as follows

$$\boldsymbol{I}_r^{\alpha\beta r}=\boldsymbol{I}_{r+}^{dq+}e^{js\omega_1 t}+\boldsymbol{I}_{r-}^{dq-}e^{-j(2-s)\omega_1 t}+\boldsymbol{I}'^{\alpha\beta}_{r}e^{-\frac{t}{T_{eqs}}}e^{-j\omega_r t}+\boldsymbol{I}'^{\alpha\beta r}_{r}e^{-\frac{t}{T_{eqr}}} \quad (47)$$

To help calculate the currents directly from the voltage characteristics, the expressions are reorganized in Table I.

TABLE I. ANALYTICAL EXPRESSIONS OF STATOR AND ROTOR CURRENTS

$\boldsymbol{I}_s^{\alpha\beta}=\frac{\boldsymbol{U}_{s+\text{ post}}^{dq+}}{j\omega_1\boldsymbol{L}_{eqs+}}e^{j\omega_1 t}-\frac{\boldsymbol{U}_{s-\text{ post}}^{dq-}}{j\omega_1\boldsymbol{L}_{eqs-}}e^{-j\omega_1 t}+\frac{\boldsymbol{U}_{s+\text{ pre}}^{dq+}-\boldsymbol{U}_{s+\text{ post}}^{dq+}+\boldsymbol{U}_{s-\text{ post}}^{dq-}}{j\omega_1\boldsymbol{L}'_{eqs}}e^{-\frac{t}{T_{eqs}}}$ $+(\boldsymbol{I}_{s+\text{ pre}}^{dq+}-\frac{\boldsymbol{U}_{s+\text{ post}}^{dq+}}{j\omega_1\boldsymbol{L}_{eqs+}}+\frac{\boldsymbol{U}_{s-\text{ post}}^{dq-}}{j\omega_1\boldsymbol{L}_{eqs-}}-\frac{\boldsymbol{U}_{s+\text{ pre}}^{dq+}-\boldsymbol{U}_{s+\text{ post}}^{dq+}+\boldsymbol{U}_{s-\text{ post}}^{dq-}}{j\omega_1\boldsymbol{L}'_{eqs}})e^{-\frac{t}{T_{eqr}}+j\omega_r t}$
$\boldsymbol{I}_r^{\alpha\beta r}=(1-\frac{L_s}{\boldsymbol{L}_{eqs+}})\frac{\boldsymbol{U}_{s+\text{ post}}^{dq+}}{j\omega_1 L_m}e^{js\omega_1 t}-(1-\frac{L_s}{\boldsymbol{L}_{eqs-}})\frac{\boldsymbol{U}_{s-\text{ post}}^{dq-}}{j\omega_1 L_m}e^{-j(2-s)\omega_1 t}$ $+(1-\frac{L_s}{\boldsymbol{L}'_{eqs}})(\frac{\boldsymbol{U}_{s+\text{ pre}}^{dq+}-\boldsymbol{U}_{s+\text{ post}}^{dq+}+\boldsymbol{U}_{s-\text{ post}}^{dq-}}{j\omega_1 L_m})e^{-\frac{t}{T_{eqs}}}e^{-j\omega_r t}$ $-\frac{L_s}{L_m}(\boldsymbol{I}_{s+\text{ pre}}^{dq+}-\frac{\boldsymbol{U}_{s+\text{ post}}^{dq+}}{j\omega_1\boldsymbol{L}_{eqs+}}+\frac{\boldsymbol{U}_{s-\text{ post}}^{dq-}}{j\omega_1\boldsymbol{L}_{eqs-}}-\frac{\boldsymbol{U}_{s+\text{ pre}}^{dq+}-\boldsymbol{U}_{s+\text{ post}}^{dq+}+\boldsymbol{U}_{s-\text{ post}}^{dq-}}{j\omega_1\boldsymbol{L}'_{eqs}})e^{-\frac{t}{T_{eqr}}}$

Finally, the three-phase stator and rotor currents can be obtained by using the Clarke transformation

$$\begin{bmatrix}i_a\\ i_b\\ i_c\end{bmatrix}=\begin{bmatrix}1 & 0\\ -1/2 & \sqrt{3}/2\\ -1/2 & -\sqrt{3}/2\end{bmatrix}\cdot\begin{bmatrix}i_\alpha\\ i_\beta\end{bmatrix} \quad (48)$$

V. VALIDATION

To validate the analytical expressions of the stator and rotor currents proposed in Section IV, this section uses a detailed EMT model of a 1.5 MW DFIG-based WTG [20] and then compare the analytical and simulation results under a common asymmetrical voltage dip scenario triggering crowbar protection.

A. Test System and Asymmetrical Voltage Dip Scenario

The parameters of the studied DFIG-based WTG are listed in Table II. Before the voltage dip occurs, the DFIG-based WTG initially operates at the rated active power (slip is -0.2) and unity power factor. The asymmetrical voltage dip occurs

at 0.5 s. The positive-sequence voltage magnitude dips from 1 pu to 0.5 pu associated with a phase angle jump of $-\pi/4$ rad. Meanwhile, the negative-sequence voltage magnitude steps up from 0 pu to 0.3 pu, and the phase angle of the negative-sequence voltage at 0.5 s is $\pi/6$ rad.

TABLE II. PARAMETERS OF A 1.5MW DFIG-BASE WTG

Parameter	Value	Parameter	Value
Voltage base for pu	563.383 V	Turns ratio	3:1
Rated active power	1.5 MW	DC link voltage	1150 V
Power base for pu	1.667 MVA	P^*	0.9 pu
R_s	0.023 pu	Q^*	0 pu
R_r	0.016 pu	$\omega_1 L_s$	3.08 pu
R_{cb}	0.097 pu (0.25Ω)	$\omega_1 L_r$	3.06 pu
ω_1	120π rad/s	$\omega_1 L_m$	2.9 pu

B. Comparisons

By substituting the voltage dip characteristics and DFIG parameters into Table I, the stator and rotor currents can be directly traced. The analytical and simulation results for the stator current are compared in Fig. 4. The comparisons for the simulated and computed rotor currents are shown in Fig. 5.

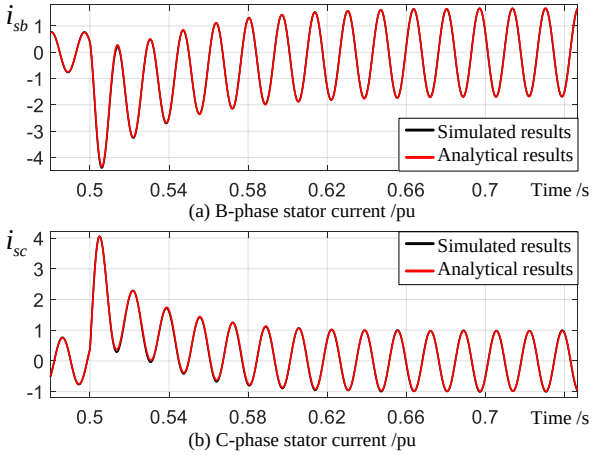

Figure 4. Comparisons between analytical and simulation results of phase-B and phase-C stator currents.

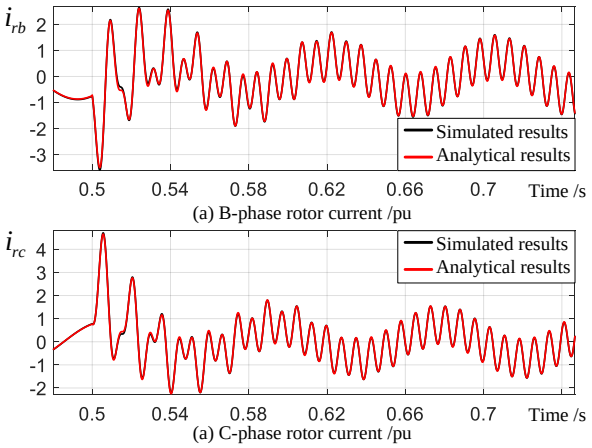

Figure 5. Comparisons between analytical and simulation results of phase-B and phase-C rotor currents.

The analytical results match the simulation results well and demonstrate how the proposed analytical expressions are accurate enough to compute transient components necessary for breaker sizing and designing the crowbar circuit.

C. Current Components

Based on the proposed analytical expressions in Table I, the characteristics of each component of the stator and rotor currents can be estimated, as shown in Fig. 6 and Fig. 7.

As shown in Fig. 6, following an asymmetrical voltage dip, the stator current is composed of two steady-state components and two transient components. The magnitudes of the positive- and negative-sequence components are constant during the voltage dip, while the DC and rotor frequency transient components gradually decay to zero.

As shown in Fig. 7, the rotor current measured at the rotor winding ports are also composed of two steady-state components and two transient components.

The magnitudes and time constants of current components can be directly used to calculate the maximal making and breaking currents for rating AC breakers [25] and crowbar resistor. Moreover, the magnitude and phase angle of the positive- and negative-sequence current components can be used to tune relay settings.

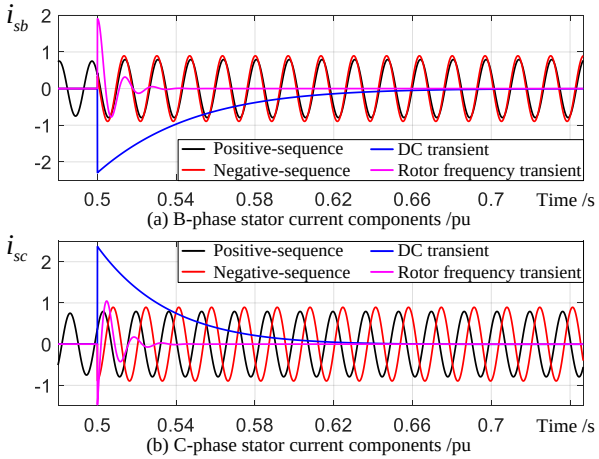

Figure 6. Components of phase-B and phase-C stator currents.

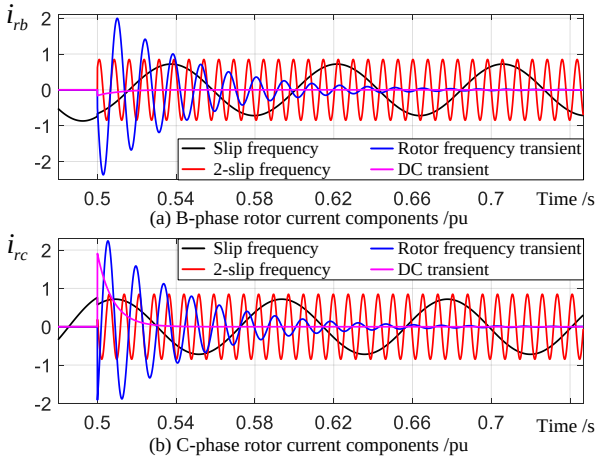

Figure 7. Components of phase-B and phase-C rotor currents.

VI. CONCLUSIONS

Asymmetrical voltage dips due to faults on the grid result in stringent operating conditions for the operation of DFIG-based WTGs. It is likely that the crowbar circuit triggers to protect the non-full-size converters. This paper has proposed concise expressions for the stator and rotor currents of DFIG-based WTGs under crowbar protection. The variations in both magnitude and angle are considered for the positive- and negative-sequence stator voltages. The characteristics of all the stator and rotor current components are estimated using the concept of equivalent stator inductance. The simplified analytical expressions can be advantageously used for power system protection studies and FRT designs. The main conclusions are summarized as follows:

(1) Before and after asymmetrical faults, the stator voltage of the DFIG can be generally characterized by the pre-fault and post-fault magnitudes and phase angles of the positive- and negative-sequence voltages. At the instant of a dip, not only the magnitudes but also the phase angles of the voltages change abruptly.

(2) For transient studies, the DFIG can be modeled with the algebraic and differential equations governing its equivalent magnetic and electric circuits. Due to the electromagnetic coupling, finding an analytical solution to these differential equations is complex. This paper proposes the use of equivalent stator inductances to convert the differential equations into algebraic equations which allows approximately obtaining the currents.

(3) The existing analytical expressions for the fault response of DFIG-based WTGs do not account for the jump in phase angle due to fault inception. The proposed expressions fully consider the steep variations in both magnitude and angle for the positive- and negative-sequence voltage vectors. The transient, positive- and negative-sequence equivalent inductances are analytically derived. This enables estimating all the current components in terms of magnitude, phase angle, time constant and frequency. Comparisons with time domain simulations performed using a detailed model of a 1.5 MW DFIG WTG show the accuracy of the proposed expressions.

(4) During asymmetrical voltage dips, the stator and rotor currents are all composed of two steady-state components and two transient components. Apart from the positive- and negative-sequence components, a DC transient component and a rotor frequency transient component will be present at the stator ports. Analytical formulations of these components can be used to understand the dynamic performance of protection elements. The analytical expressions of transient rotor current can be used to rate the crowbar circuit and design its operating/releasing criteria in an efficient manner.

REFERENCES

[1] A. Haddadi, E. Farantatos, I. Kocar, and U. Karaagac, "Impact of Inverter Based Resources on System Protection," *Energies*, vol. 14, no. 4, p. 1050, Feb. 2021.

[2] A. Haddadi, I. Kocar, J. Mahseredjian, U. Karaagac and E. Farantatos, "Performance of Phase Comparison Line Protection Under Inverter-Based Resources and Impact of the German Grid Code," *2020 IEEE Power & Energy Society General Meeting (PESGM)*, Montreal, QC, Canada, 2020, pp. 1-5.

[3] K. El-Arroudi and G. Joós, "Performance of Interconnection Protection Based on Distance Relaying for Wind Power Distributed Generation," in *IEEE Transactions on Power Delivery*, vol. 33, no. 2, pp. 620-629, April 2018.

[4] Y. Chang, J. Hu, G. Song, X. Kong and Y. Yuan, "Impact of DFIG-based wind turbine's fault current on distance relay during symmetrical faults," in *IET Renewable Power Generation*, vol. 14, no. 66, pp. 3097-3102, Dec. 2020.

[5] G. Pannell, D. J. Atkinson and B. Zahawi, "Minimum-Threshold Crowbar for a Fault-Ride-Through Grid-Code-Compliant DFIG Wind Turbine," in *IEEE Transactions on Energy Conversion*, vol. 25, no. 3, pp. 750-759, Sept. 2010.

[6] S. Hu, X. Zou and Y. Kang, "A novel optimal design of DFIG crowbar resistor during grid faults," *2014 International Power Electronics Conference (IPEC-Hiroshima 2014 - ECCE ASIA)*, Hiroshima, Japan, 2014, pp. 555-559.

[7] G. Abad, J. Lopez, M. A. Rodriguez, L. Marroyo and G. Iwanski, "Analysis of The DFIM under Voltage Dips," in *Doubly Fed Induction Machine: Modeling and Control for Wind Energy Generation Applications*, 1, Wiley-IEEE Press, 2011, pp.278-291.

[8] S. Engelhardt, J. Kretschmann, J. Fortmann, F. Shewarega, I. Erlich and T. Neumann, "Capability and limitations of DFIG based wind turbines concerning negative sequence control," *2013 IEEE Power & Energy Society General Meeting*, Vancouver, BC, Canada, 2013, pp. 1-5.

[9] A. K. Elnaggar, J. L. Rueda and I. Erlich, "Comparison of short-circuit current contribution of Doubly-Fed induction generator-based wind turbines and synchronous generator," *2013 IEEE Grenoble Conference*, Grenoble, 2013, pp. 1-6.

[10] E. Muljadi and V. Gevorgian, "Short-circuit modeling of a wind power plant," *2011 IEEE Power and Energy Society General Meeting*, San Diego, CA, 2011, pp. 1-9.

[11] A. El-Naggar and I. Erlich, "Fault Current Contribution Analysis of Doubly Fed Induction Generator-Based Wind Turbines," in *IEEE Transactions on Energy Conversion*, vol. 30, no. 3, pp. 874-882, Sept. 2015.

[12] J. Morren and S. W. H. de Haan, "Short-Circuit Current of Wind Turbines with Doubly Fed Induction Generator," in *IEEE Transactions on Energy Conversion*, vol. 22, no. 1, pp. 174-180, March 2007.

[13] G. Pannell, D. J. Atkinson and B. Zahawi, "Analytical Study of Grid-Fault Response of Wind Turbine Doubly Fed Induction Generator," in *IEEE Transactions on Energy Conversion*, vol. 25, no. 4, pp. 1081-1091, Dec. 2010.

[14] Y. Chang, J. Hu and X. Yuan, "Mechanism Analysis of DFIG-Based Wind Turbine's Fault Current During LVRT With Equivalent Inductances," in *IEEE Journal of Emerging and Selected Topics in Power Electronics*, vol. 8, no. 2, pp. 1515-1527, June 2020.

[15] A. Marmolejo, M. Palazzo and M. Delfanti, "Short-circuit current of a doubly-fed induction generator: Analytical solution and insights," *2014 IEEE Conference on Energy Conversion (CENCON)*, Johor Bahru, Malaysia, 2014, pp. 128-133.

[16] F. Sulla, J. Svensson and O. Samuelsson, "Symmetrical and unsymmetrical short-circuit current of squirrel-cage and doubly-fed induction generators," in *Electric Power Systems Research*, 81(7), pp. 1610-1618, 2011.

[17] S. Yang, T. Zhou, L. Chang, Z. Xie and X. Zhang, "Analytical Method for DFIG Transients During Voltage Dips," in *IEEE Transactions on Power Electronics*, vol. 32, no. 9, pp. 6863-6881, Sept. 2017.

[18] F. Xiao, Z. Zhang and X. Yin, "Fault Current Characteristics of the DFIG under Asymmetrical Fault Conditions," in *Energies*, vol. 2015, no. 8, pp. 10971-10992, 2015.

[19] X. Yu, Y. Chang, J. Hu and L. Shang, "Fault Current Analysis of Type-3 Wind Turbine Considering Dynamic Influence of Phase Locked Loop," *2019 10th International Conference on Power Electronics and ECCE Asia (ICPE 2019 - ECCE Asia)*, Busan, Korea (South), 2019, pp. 2899-2904.

[20] A. Haddadi, I. Kocar, T. Kauffmann, U. Karaagac, E. Farantatos and J. Mahseredjian, "Field validation of generic wind park models using fault records," in *Journal of Modern Power Systems and Clean Energy*, vol. 7, no. 4, pp. 826-836, July 2019.
[21] J. Pyrhonen, V. Hrabovcová, S. R. Semken, "Fundamentals of Space-vector Theory," in *Electrical Machine Drives Control: An Introduction: An Introduction*, 1, Wiley-IEEE Press, 2016, pp.66-90.
[22] Y. Chang, I. Kocar, J. Hu, U. Karaagac, K. W. Chan and J. Mahseredjian, "Coordinated Control of DFIG Converters to Comply with Reactive Current Requirements in Emerging Grid Codes," in *Journal of Modern Power Systems and Clean Energy*, vol. 10, no. 2, pp. 502-514, March 2022.
[23] Math H. Bollen, "Voltage sags-characterization," in *Understanding Power Quality Problems: Voltage Sags and Interruptions*, 1, Wiley-IEEE Press, 2000, pp.139-251.
[24] J. Lopez, P. Sanchis, X. Roboam and L. Marroyo, "Dynamic Behavior of the Doubly Fed Induction Generator During Three-Phase Voltage Dips," in *IEEE Transactions on Energy Conversion*, vol. 22, no. 3, pp. 709-717, Sept. 2007.
[25] High-voltage switchgear and controlgear – Part 100: Alternating-current-breakers, IEC Standard 62271-100, June. 2017.